Supplementary Fig. 1

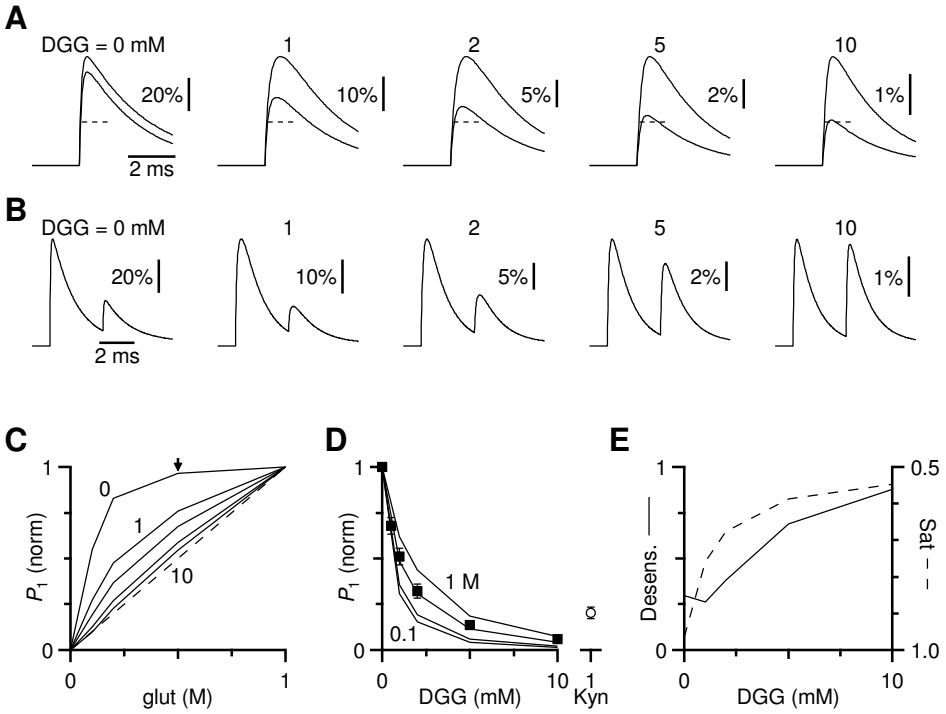

Supplementary Fig. 2

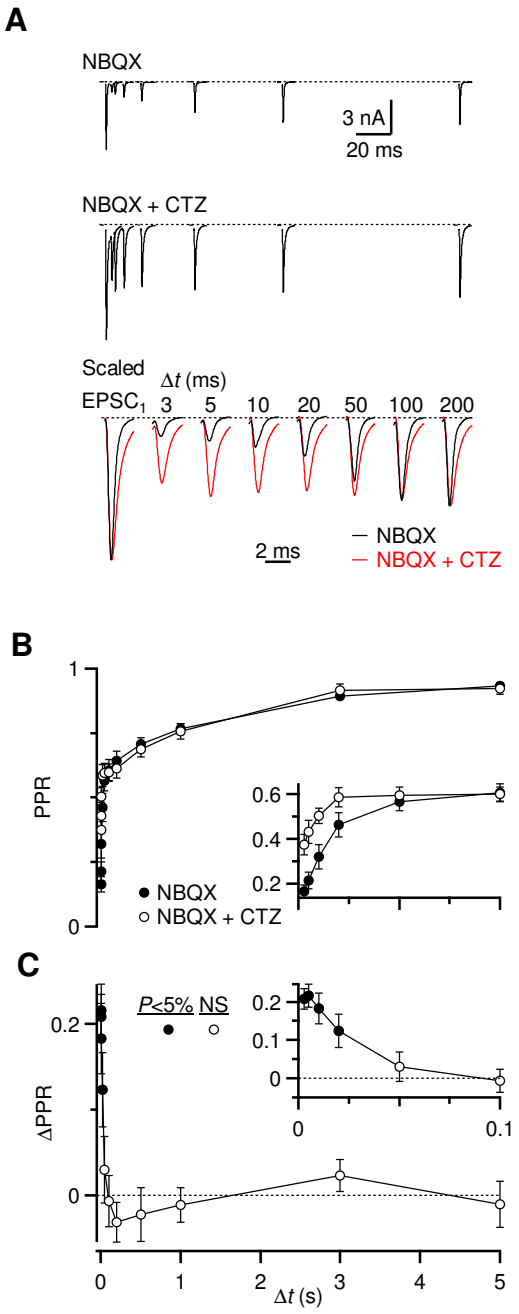

Supplementary Fig. 3

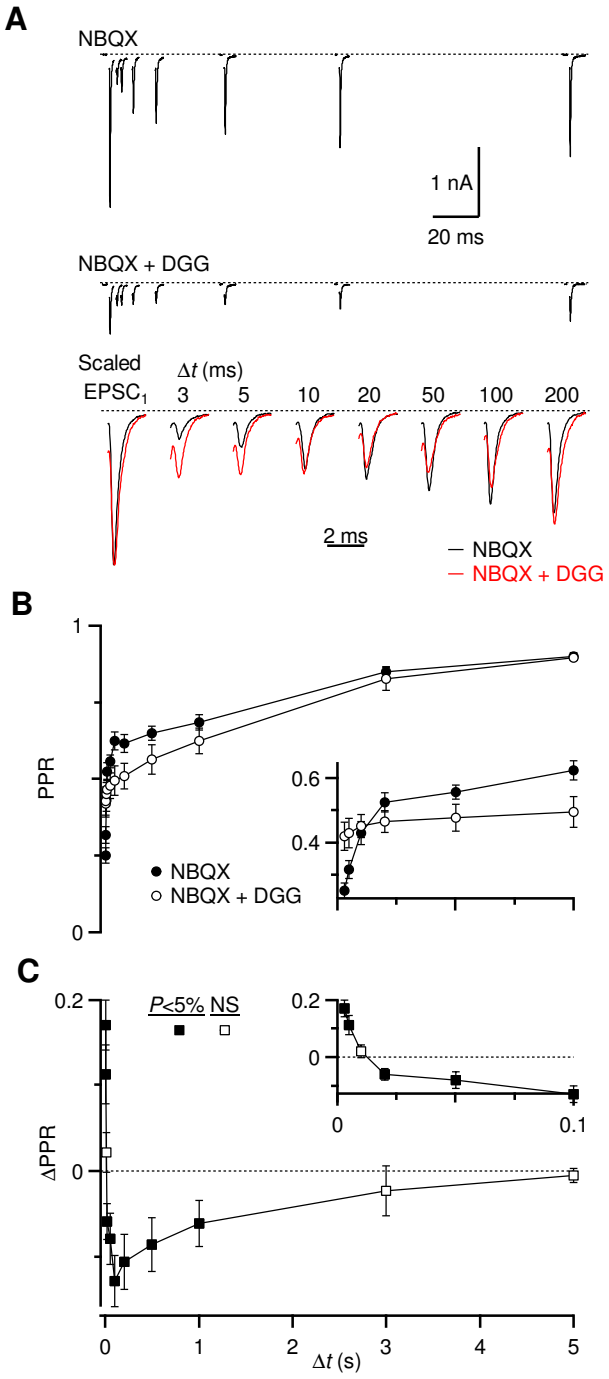

Supplementary Fig. 4

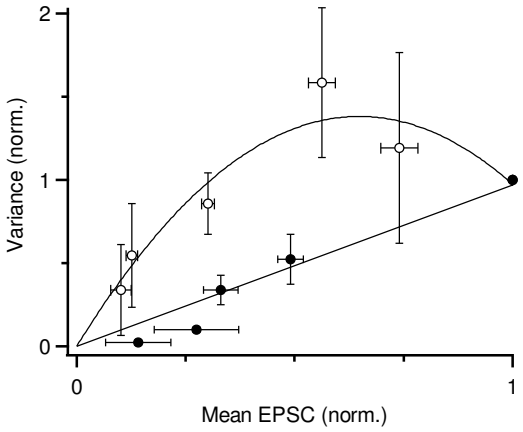

Supplementary Fig. 5

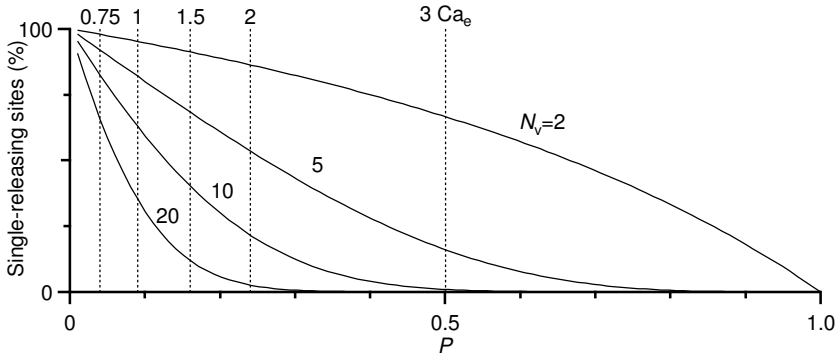

Supplementary Figure 1. DGG reduces the effects of both desensitization and saturation in parallel.

A. Open probability of modelled AMPARs in response to pulses of glutamate (200 or 500 mM) in the presence of DGG (0, 1, 2, 5, or 10 mM). The dashed line in each pair of traces is at 40% of the peak for the 500 mM glutamate pulse, which is the linear prediction for a 200 mM glutamate pulse. The linear prediction was achieved with 5 and 10 mM DGG (right traces).

B. Responses of modelled AMPARs to pairs of 500 mM glutamate pulses in different concentrations of DGG. The response to the second pulse is nearly equal to the first in 10 mM DGG, indicating that desensitization has been prevented.

C. DGG at high concentrations causes AMPARs to report glutamate concentration in a linear fashion. Simulations similar to part A are normalized to the response to a 1 M glutamate pulse. Solid lines track the peak open probability (P_1) as a function of glutamate pulse amplitude. Each line is in a different DGG concentration (from 0 to 10 mM). In 0 DGG, the response is highly saturated, with large changes in P_1 up to 200 mM glutamate, but smaller changes above that. With increasing DGG, the response becomes closer to linear (dashed line). The arrow indicates the data that are plotted in the dashed line of panel E.

D. Block of the AMPAR response by DGG. Solid lines track P_1, as a function of DGG concentration. Each line is a different glutamate pulse amplitude (from 0.1 to 1 M). Block was normalized to P_1 in 0 DGG. Markers show experimental data from Fig. 3 for the effects of DGG on endbulb EPSCs (solid squares), indicating that the 500 mM glutamate pulse most closely mimics the behavior of the endbulb. Because this model was not based on endbulbs, we do not claim that 500 mM is the actual glutamate concentration at the endbulb. However, pulses of 500 mM glutamate within this model provide a useful point for qualitative comparison with endbulb EPSCs. The relative block by 1 mM kynurenate (open circle) is included for comparison.

E. DGG affects both desensitization and saturation to similar extents at each concentration. To represent desensitization (solid line), we normalized the open probability resulting from the second pulse of glutamate (P_2) relative to P_1 for pairs of 500 mM glutamate pulses (panel B). This differs from the paired-pulse ratio for synaptic

stimulation, because here the glutamate pulses are equal. To represent saturation (dashed line) we normalized P_1 for a 500 mM pulse of glutamate to the peak P_1 for a 1 M pulse. A normalized value of 0.5 represents a linear response, and saturated responses should approach 1. These data are also indicated by the arrow in panel C. The axis is flipped to facilitate comparison with the effects of DGG on desensitization. This plot demonstrates that the two effects of DGG on saturation and desensitization take place in parallel and cannot be simply separated, for example by choosing different concentrations of DGG.

Modelling: The glutamate transient was modelled as diffusion of a disk of glutamate at the point of release, given by the equation $C(t) = C_0\left[1 - \exp\left(-\frac{\rho^2}{4dt}\right)\right]$, where C_0 is the starting concentration, ρ is the vesicle radius (25 nm), d is the diffusion constant (0.4 μm^2/ms). Parameters for the AMPAR model are detailed in (Wadiche and Jahr 2001). Although this model was based on Purkinje cell AMPARs, we used it because it incorporated kinetic parameters related to DGG binding, and would therefore provide insight into the effects of DGG on saturation and desensitization. Simulations were done by Euler integration with a step size of 0.2 μs using Wavemetrics Igor.

Supplementary Figure 2. Effect of CTZ on PPR in the presence of NBQX.
CTZ was applied in the presence of NBQX, and PPR at different Δt values were compared. *A*: Example EPSC traces in NBQX (*upper panel*) and in NBQX + CTZ (*middle panel*). The lower panel shows NBQX and NBQX + CTZ traces scaled to the amplitude of $EPSC_1$. *B*: Average results for 9 endbulbs. The insets expand the intervals Δt = 3 to 100 ms. *C*: The ΔPPR is shown. Filled markers indicate intervals that are significantly above 0 ($P < 0.05$).

Supplementary Figure 3. Effect of DGG on PPR in the presence of NBQX.
DGG was applied in the presence of NBQX, and PPR at different Δt values were compared. *A*: Example EPSC traces in NBQX (*upper panel*) and in NBQX + DGG (*middle panel*). The lower panel shows NBQX and NBQX + DGG traces scaled to the amplitude of $EPSC_1$. *B*: Average results for 7 endbulbs. The insets expand the intervals

Δt = 3 to 100 ms. *C*: The ΔPPR is shown. Filled markers indicate intervals that differ significantly from 0 ($P < 0.05$).

Supplementary Fig. 4. Mean-variance analysis. We estimated the probability of release using mean-variance analysis (Silver 2003). To summarize the approach, the EPSC mean (μ) and variance (σ^2) are measured under various conditions, and the results are plotted. Under the binomial model of release, $\mu = NPq$, and $\sigma^2 = NP(1 - P)q^2$, where q is the quantal size, N is related to the number of released vesicles, and P is the probability of release. Thus, the variance is 0 when $P = 0$ and $P = 1$, and it reaches a maximum when $P = 0.5$. When P is varied by changing Ca_e, substituting yields the relationship: $\sigma^2 = q\mu - \mu^2/N$. Thus a fit to the observed mean and variance directly yields N and q, and P can then be calculated for different μ. When saturation is high, N and P better reflect the behavior of release sites, whereas when saturation is low, these better reflect the number of releasable vesicles (N_v) and the probability of vesicle release (Foster and Regehr 2004). This approach has been applied to the endbulb to examine the behavior of release sites (Oleskevich et al. 2000)(Wang & Manis 2005).

We found similar effects on the mean and variance when we varied Ca_e for 11 cells in the absence of DGG (open symbols). To better compare between experiments, we normalized the mean and variance to the values in 3 Ca_e and averaged data together for each Ca_e. Each point is the average of 4 to 11 experiments. A fit to these data yielded an estimate of P for a release site of 0.57 in 2 Ca_e, which is similar to previous estimates.

To estimate the probability of vesicle release, we applied this approach to the results of similar experiments conducted in the presence of DGG (closed symbols). Each point is the average of 4 to 9 cells. We found that the variance only increased with Ca_e, and did not decrease in any of the 9 experiments. This means that it is not possible to fit the data using the relationship described above. However, we can use the fact that the variance reaches a maximum when $P = 0.5$ to conclude, at least, that P in 3 $Ca_e < 0.5$. We use this to place upper bounds on P in different Ca_e, as described in the Discussion.

Supplementary Fig. 5. Single vs. multivesicular release under the binomial model. To evaluate whether the changes in block by DGG at very low Ca_e are explainable by changes in the amount of multivesicular vs. single vesicle release, we used the binomial model of release. The percentage of neurotransmitter-releasing sites that only release a single vesicle is given by the relationship:

$$\begin{aligned}\%_{\text{single}} &= 100\% \times p_1 / \sum_{k=1}^{N_v} p_k \\ &= 100\% \times p_1 / (1 - p_0) \\ &= 100\% \times N_v P (1 - P)^{N_v - 1} / [1 - (1 - P)^{N_v}],\end{aligned}$$

where p_k is the binomial probability of releasing k vesicles, P is the probability of vesicle release, and N_v is the number of releasable vesicles at a given site. This quantity should be related to the effectiveness of DGG: DGG should block more effectively when $\%_{\text{single}}$ is high than when $\%_{\text{single}}$ is low.

The figure shows this equation evaluated over a range of P and N_v. The vertical grid marks indicate the upper-bound estimates we have made on P for the different Ca_e conditions (see Supp. Fig. 3 and Discussion). This figure shows that $\%_{\text{single}}$ is significantly less than 100% (i.e. there is considerable multivesicular release) even when P is low. Furthermore, $\%_{\text{single}}$ changes significantly as P increases. This means that DGG should show measurably different effects at different, low Ca_e. This is fully consistent with our observations in Fig. 3.